

Frequency-Secured Unit Commitment: Tight Approximation using Bernstein Polynomials

Bo Zhou, *Member, IEEE*, Ruiwei Jiang, *Member, IEEE*, and Siqian Shen

Abstract—As we replace conventional synchronous generators with renewable energy, the frequency security of power systems is at higher risk. This calls for a more careful consideration of unit commitment (UC) and primary frequency response (PFR) reserves. This paper studies frequency-secured UC under significant wind power uncertainty. We coordinate the thermal units and wind farms to provide frequency support, wherein we optimize the variable inverter droop factors of the wind farms for higher economy. In addition, we adopt distributionally robust chance constraints (DRCCs) to handle the wind power uncertainty. To depict the frequency dynamics, we incorporate a differential-algebraic equation (DAE) with the dead band into the UC model. Notably, we apply Bernstein polynomials to derive tight inner approximation of the DAE and obtain mixed-integer linear constraints, which can be computed in off-the-shelf solvers. Case studies demonstrate the tightness and effectiveness of the proposed method in guaranteeing frequency security.

Index Terms—Unit commitment, frequency security, differential-algebraic equation, Bernstein polynomial, variable droop factors, distributionally robust chance constraint

NOMENCLATURE

Abbreviations

BP	Bernstein polynomial
DAE	differential-algebraic equation
DRCC	distributionally robust chance constraint
PFR	primary frequency response
QSS	quasi-steady-state
RoCoF	rate of change of frequency
SFR	system frequency response
UC	unit commitment

Indices

τ	period index
τ'	segment index
i	bus index
j	line index
t	time instant

Parameters

Δf_{DB}	dead band
ΔP_d	power imbalance
ε	risk threshold
$\overline{\Delta f}_{err}$	max. admitted frequency deviation at the QSS
$\overline{\Delta f}$	max. admitted frequency deviation at the nadir
$\overline{\dot{f}}$	max. admitted RoCoF
$\overline{G}_w/\underline{G}_w$	max./min. values of the inverter droop factors

\overline{P}_g/P_g	max./min. power generation of thermal units
P_l	line capacity limit
c_g^{PR}/c_w^{PR}	unit reserve cost of thermal units/wind farms
c_{su}/c_{sd}	start-up/shut-down cost
G_g	droop factor of thermal units
$h_{\tau'}$	time length of segment τ'
H_g	inertia constant of thermal units
H_w	inertia constant of wind farms
k_D	load damping rate
P_d	power load
r_{su}/r_{sd}	max. power generation at start-up/shut-down
r_u/r_d	upward/downward ramping limit
S	power transfer distribution factors
T_{on}/T_{off}	min. up/down time of thermal units
T_g	response constant of governors
T_w	response constant of inverters

Variables

$[\Delta f]$	frequency deviation
F_g	fuel cost of thermal units
G_w	droop factor of wind farms
H_{sys}	total inertia
I_g	online/offline status of thermal units
P_w^A/P_w	available/integrated power of wind farms
P_g^{PR}	PFR power from thermal units
P_{sys}^{PR}	total PFR power
P_w^{PR}	PFR power from wind farms
P_g	power generation of thermal units
P_g^{PR}	generation segment of thermal units
R_g^{PR}/R_w^{PR}	PFR reserves of thermal units/wind farms
U_g/D_g	start-up/shut-down actions of thermal units

I. INTRODUCTION

THE energy and climate crisis has motivated sustainable development and an explosive increase of renewable energy use worldwide [1]. However, the significant integration of renewables brings many challenges. Among them, frequency security has drawn increasing attention [2]. Different from synchronous thermal units that have rotators and governors, renewable generation is usually controlled by inverters, which cannot provide rotational inertia and primary frequency response (PFR) under the typical maximum power point tracking mode [3]. As renewables gradually replace thermal units, the total rotational inertia and PFR capacity in the power system decrease. Consequently, when a sudden power imbalance occurs, the system frequency will change more sharply and deviate from the nominal frequency more drastically, threatening the frequency security.

A significant amount of effort has been devoted to frequency security under a high share of renewables. Straightforwardly,

Ruiwei Jiang was supported in part by the U.S. National Science Foundation under Grant ECCS-1845980. Bo Zhou and Siqian Shen were supported in part by the U.S. Department of Energy, Grant #DE-SC0018018. (Corresponding author: Bo Zhou, email: bozum@umich.edu)

The authors are with the Department of Industrial and Operations Engineering, University of Michigan, Ann Arbor, MI 48109, USA.

one can keep sufficient synchronous units online, yet this may induce large curtailment of renewables. Some prior works considered emergency resources for frequency support, such as energy storage [4] and HVDC links [5]. However, these approaches incur either high investment or operational risks. Fortunately, modern development of control technologies has allowed renewables themselves to contribute to frequency support [6]. Using proper control strategies, renewables can adjust their integrated power according to frequency deviation and provide virtual inertia and PFR capacity [7]. This is relatively cheaper and more practical as the integration of renewables further increases. As a result, renewable generation is becoming an important resource that can be coordinated with thermal units to guarantee frequency security.

Nevertheless, providing frequency support changes the operation of the power system. On the one hand, sufficient inertia is required to depress sharp frequency variations, and hence, more units may need to be put online [8]. On the other hand, sufficient PFR reserves are required for effective real-time PFR, for which thermal units need to reserve some generation capacity [9] and renewable generation will be operated under the deloaded mode [10]. Both the above changes will increase the operational cost, yet they are coupled to influence frequency dynamics and further affect frequency security. Therefore, it is of high significance to carefully decide unit commitment (UC) and PFR reserves, in order to maintain frequency security in an economic manner.

There have been many significant works that considered frequency security in scheduling, such as economic dispatch [11], UC [12], [13], and energy market [14]. However, due to the complex coupling of frequency dynamics, various frequency support resources, and the uncertainty of renewables, it remains challenging to compute frequency-secured UC accurately and tractably, which is the research focus of this paper.

To guarantee frequency security, three metrics of frequency dynamics are usually considered, including the rate of change of frequency (RoCoF), the frequency nadir, and the quasi-steady-state (QSS) frequency deviation [15], [16]. Unfortunately, these metrics are difficult to calculate because frequency dynamics are governed by a series of differential-algebraic equations (DAEs) [17]. Additionally, the dead band, which is utilized to avoid frequent PFR and to reduce the maintenance cost of governors, needs to be considered and further complicates the calculation [18], [19]. Much effort has been devoted to simulating or approximating frequency dynamics. First, numerical simulation tools (such as Simulink) can accurately evaluate frequency dynamics, but these methods are computationally heavy and intractable to incorporate into optimization models. Second, existing studies mainly adopt the system frequency response (SFR) model, through which frequency dynamics and its nadir can be analytically derived [20], [21]. Unfortunately, this analytical expression of nadir is intractable even when the dead band is ignored. Third, some studies simplify the derivation by assuming a linear ramping model for PFR, wherein the dead band is considered [22], [23]. However, such simplification ignores PFR dynamics and induces low accuracy. Moreover, this approach results in a highly nonlinear expression for the

frequency nadir. Finally, various approximation methods have been developed to linearize the expression [20], [24], [25] or to obtain inner approximations [21]–[23], most of which are unfortunately conservative and sacrifice the economy. In this paper, we propose to adopt a novel inner approximation based on the Bernstein polynomials (BPs). This approach leads to a tight approximation and can be incorporated into the UC model more tractably.

As important frequency support resources, renewable generation is uncertain, which strongly impacts PFR capacities and frequency dynamics. In what follows, we consider wind power uncertainties for example [26] and the same approach adapts to other renewables. Due to wind uncertainties, the real-time available wind generation may be different from the day-ahead forecast that is used to decide the PFR reserves of wind farms. If the available wind generation is less than the required PFR reserves, PFR capacities from wind farms will be limited and cannot play the expected role, resulting in a larger frequency deviation and threatening frequency security [9], [10]. Two approaches can help address this issue. On the one hand, the frequency-secured UC model can explicitly incorporate the wind uncertainties using, e.g., stochastic approximation [21], chance constraints [22], [23], [27]–[29], and robust optimization [30]. In this paper, we adopt distributionally robust chance constraints (DRCCs) in view of their tractability and good out-of-sample performance [31]–[33]. On the other hand, we can adjust the PFR reserves across time, e.g., through the droop factors used in the control strategy of the wind farm inverters [34], to adapt to the varying wind generation. Variable droop factors can also help to better coordinate thermal units and wind farms in providing frequency support and enhancing the operational economy.

Our main contributions are summarized as follows.

- 1) We propose a frequency-secured UC model to accommodate under-frequency events, where thermal units and wind farms are coordinated to provide frequency support. DRCCs and variable droop factors are employed to handle the wind power uncertainty.
- 2) We incorporate frequency dynamic DAEs into the UC model and consider the dead band. To alleviate the computational challenge, we derive a tight inner approximation using BPs. This transforms the DAEs as mixed-integer linear constraints, which can be computed by off-the-shelf optimization solvers. In addition, we recast the DRCCs as linear constraints, which can be computed efficiently.
- 3) Through extensive case studies, we demonstrate the tightness of the BP approximation, the necessity of considering the dead band, the value of using variable droop factors of the wind farms, and the scalability of our approach.

The remainder of this paper is organized as follows. Section II establishes the problem formulation of frequency-secured UC under wind power uncertainty. Section III derives the BP approximation of frequency dynamics DAEs and a tractable reformulation of the DRCCs. Case studies are conducted in Section IV and conclusions are drawn in Section V.

II. PROBLEM FORMULATION

We first introduce the general process of frequency dynamics, then propose the DAE frequency security constraints, and finally formulate a frequency-secured UC model.

A. Frequency Dynamics

Fig. 1 depicts a general process of frequency dynamics under a sudden loss of generation at time t_0 . At the beginning (time t_0-t_{DB}), before the frequency deviation exceeds the dead band Δf_{DB} , the governors do not work and inertia plays the whole role in mitigating the frequency drop. Generally, the maximum RoCoF occurs at t_0 . As the frequency deviation exceeds Δf_{DB} , the governors start working, and PFR becomes significant (time $t_{DB}-t_{QSS}$), the frequency eventually reaches a QSS with deviation Δf_{QSS} . During the whole dynamics, frequency first drops and is then lifted, yielding a nadir with deviation Δf_{nadir} at t_{nadir} .

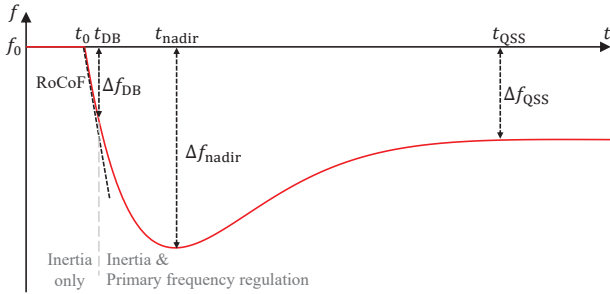


Fig. 1. A general process of the frequency dynamics

B. DAE Frequency Security Constraints

We depict the SFR model [17] of frequency dynamics in Fig. 2. In this model, ΔP_d is the power imbalance and $\Delta f(t) = f_0 - f(t)$ is the frequency deviation from the nominal frequency f_0 at time instant t . P_{sys}^{PR} is the total PFR power in the power system, and P_g^{PR} and P_w^{PR} are the PFR power from thermal units and wind farms, respectively. To avoid frequent PFR, the governors of thermal units and inverters of wind farms will not respond to a non-zero $\Delta f(t)$ unless its magnitude exceeds the dead band Δf_{DB} .

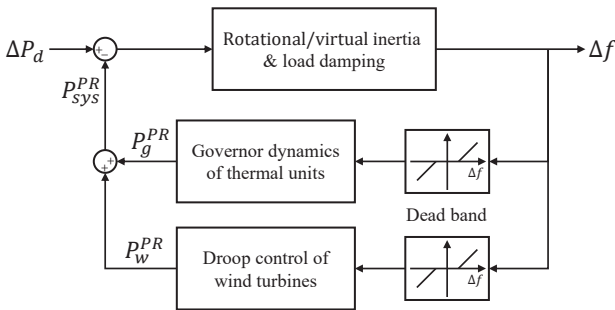


Fig. 2. SFR model considering the dead band

This divides the frequency dynamics into two stages. In the first stage, frequency deviation lies within the dead band and

so there is no PFR. As in Fig. 2, system frequency dynamics follow the governing equations

$$2H_{sys} \frac{d\Delta f(t)}{dt} + k_D P_d \Delta f(t) = \Delta P_d, \quad t \in [0, t_{DB}] \quad (1a)$$

$$\Delta f(t)|_{t=0} = 0, \quad \Delta f(t)|_{t=t_{DB}} = \Delta f_{DB}, \quad (1b)$$

where H_{sys} is the total inertia in the power system, including rotational inertia H_g from thermal units and virtual inertia H_w from wind farms, k_D is the load damping rate, and P_d is the power load. Constraint (1b) gives the initial and final conditions of the ordinary differential equation (1a). Note that t_{DB} in (1) is not a given parameter, but a variable that depends on frequency dynamics and the dead band Δf_{DB} . In the second stage, frequency deviation exceeds Δf_{DB} and PFR starts working. Accordingly, the system frequency dynamics follow the governing equations

$$2H_{sys} \frac{d\Delta f(t)}{dt} + k_D P_d \Delta f(t) = \Delta P_d - P_{sys}^{PR}(t), \quad t \geq t_{DB} \quad (2a)$$

$$\Delta f(t)|_{t=t_{DB}} = \Delta f_{DB} \quad (2b)$$

$$P_{sys}^{PR}(t) = \sum_i [P_{g,i}^{PR}(t) + P_{w,i}^{PR}(t)] \quad (3a)$$

$$T_{g,i} \frac{dP_{g,i}^{PR}(t)}{dt} + P_{g,i}^{PR}(t) = G_{g,i} I_{g,i} [\Delta f(t) - \Delta f_{DB}] \quad (3b)$$

$$P_{g,i}^{PR}(t)|_{t=t_{DB}} = 0 \quad (3c)$$

$$P_{w,i}^{PR}(t) = G_{w,i} [\Delta f(t) - \Delta f_{DB}], \quad (3d)$$

where i is the bus index, T_g is the response constant of governors, and G_g is the droop factor of thermal units. The response constant of wind power is $T_w \approx 0$ because it is controlled by inverters. G_w is the variable droop factor of wind farms, which can be adjusted to adapt to wind uncertainties and to enhance the coordination of thermal units and wind farms. Constraint (2b) gives the initial condition of the ordinary differential equation (2a). Constraint (3a) describes that the total PFR power $P_{sys}^{PR}(t)$ comes from all power sources, including thermal units and wind farms. According to the response characteristic of the governors, P_g^{PR} is described in (3b), where I_g indicates the online/offline status of thermal units ($I_g = 1$ if online and $I_g = 0$ if offline). Constraint (3c) gives the initial condition of the ordinary differential equation (3b). Finally, similar to (3b), (3d) describes the dynamics of the wind farm PFR power P_w^{PR} .

To protect frequency security, we restrict the RoCoF, nadir, and quasi-steady-state deviation as

$$\frac{d\Delta f(t)}{dt} \leq \bar{f} \quad (4a)$$

$$\Delta f(t)|_{nadir} \leq \overline{\Delta f} \quad (4b)$$

$$\Delta f(t)|_{QSS} \leq \overline{\Delta f_{err}}, \quad (4c)$$

where \bar{f} is the maximum admitted RoCoF, and $\overline{\Delta f}$ and $\overline{\Delta f_{err}}$ are the maximum admitted frequency deviation at the nadir and QSS, respectively. Note that without loss of generality, only under-frequency events are considered.

C. Frequency-Secured Chance-Constrained Unit Commitment

We formulate the following frequency-secured UC model with DAEs and DRCCs.

$$\min \sum_{\tau} \sum_i (c_{su,i} U_{g,i,\tau} + c_{sd,i} D_{g,i,\tau} + F_{g,i,\tau} + c_g^{PR} R_{g,i,\tau}^{PR} + c_w^{PR} R_{w,i,\tau}^{PR}) \quad (5)$$

$$\text{s.t. (1)–(4)} \quad (6)$$

$$\begin{cases} F_{g,i,\tau} = c_{on,i} I_{g,i,\tau} + \sum_k \lambda_{g,i,k} P_{g,i,k,\tau} \\ P_{g,i,\tau} = \underline{P}_{g,i} I_{g,i,\tau} + \sum_k P_{g,i,k,\tau} \\ 0 \leq p_{g,i,k,\tau} \leq (\overline{P}_{g,i} - \underline{P}_{g,i}) / N_{pw} \end{cases} \quad (7)$$

$$U_{g,i,\tau} + D_{g,i,\tau} \leq 1 \quad (8a)$$

$$U_{g,i,\tau} - D_{g,i,\tau} = I_{g,i,(\tau+1)} - I_{g,i,\tau} \quad (8b)$$

$$\begin{cases} \sum_{k=\tau+1}^{t+T_{on,i}} I_{g,i,k} \geq T_{on,i} U_{g,i,\tau} \\ \sum_{k=\tau+1}^{t+T_{off,i}} (1 - I_{g,i,k}) \geq T_{off,i} D_{g,i,\tau} \end{cases} \quad (8c)$$

$$H_{sys,\tau} = \sum_i (H_{g,i} I_{g,i,\tau} + H_{w,i}) \quad (9a)$$

$$\underline{G}_{w,i} \leq G_{w,i,\tau} \leq \overline{G}_{w,i} \quad (9b)$$

$$\begin{cases} P_{g,i,\tau}^{PR}(t) \leq R_{g,i,\tau}^{PR} \\ P_{w,i,\tau}^{PR}(t) \leq R_{w,i,\tau}^{PR} \end{cases} \quad (9c)$$

$$\underline{P}_{g,i} I_{g,i,\tau} \leq P_{g,i,\tau} \leq \overline{P}_{g,i} I_{g,i,\tau} - R_{g,i,\tau}^{PR} \quad (10a)$$

$$\begin{cases} P_{g,i,(\tau+1)} - P_{g,i,\tau} \leq r_{u,i} I_{g,i,\tau} + r_{su,i} U_{g,i,\tau} \\ P_{g,i,\tau} - P_{g,i,(\tau+1)} \leq r_{d,i} I_{g,i,(\tau+1)} + r_{sd,i} D_{g,i,\tau} \end{cases} \quad (10b)$$

$$\sum_i (P_{g,i,\tau} + P_{w,i,\tau}) = \sum_i P_{d,i,\tau} \quad (11)$$

$$-\overline{P}_{l,j} \leq \sum_i S_{ji} (P_{g,i,\tau} + P_{w,i,\tau} - P_{d,i,\tau}) \leq \overline{P}_{l,j} \quad (12)$$

$$\inf_{\mathbb{P} \in \mathcal{D}} \mathbb{P} \{ P_{w,i,\tau} + R_{w,i,\tau}^{PR} \leq P_{w,i,\tau}^A \} \geq 1 - \varepsilon, \quad (13)$$

where τ is the index for time periods. The objective (5) consists of start-up/shut-down cost, PFR reserve cost, and fuel cost. Binary decision variables U_g and D_g represent the start-up and shut-down actions of thermal units, respectively, and c_{su} and c_{sd} are the corresponding costs. Continuous decision variables R_g^{PR} and R_w^{PR} represent the PFR reserves of thermal units and wind farms, respectively, and c_g^{PR} and c_w^{PR} are the corresponding unit costs.

Constraints (7) formulate the fuel cost F_g of thermal units as a piecewise linear function of the amount P_g of power generation [35]. Specifically, p_g is the generation segment, N_{pw} is the piecewise number, and $\lambda_{g,k}$ is the cost incremental coefficient of the k th segment. \overline{P}_g and \underline{P}_g are the maximum and minimum power generation of thermal units, respectively. Constraints (8) formulate the UC restrictions, where T_{on} and T_{off} are minimum up and down time, respectively.

Constraints (8a)–(8b) formulate the logic among decision variables U_g , D_g , and I_g , and constraints (8c) formulate the minimum up/down time restrictions. Constraints (9) formulate the frequency security, where $\overline{G}_{w,i}$ and $\underline{G}_{w,i}$ are the maximum and minimum values of the inverter droop factor, respectively. In particular, (9a) calculates the total inertia of the power system, and (9c) ensures that the PFR power does not exceed the PFR reserve. Constraints (10) describe the ramping restrictions, where r_u/r_d is the upward/downward ramping limit and r_{su}/r_{sd} is the maximum power generation at start-up/shut-down. Constraints (11) describe the system power balance, where P_d is the power load. Constraints (12) describe the transmission line capacity limits, where j is the line index, \overline{P}_j is the line capacity limit, and S_{ji} is the power transfer distribution factor based on DC power flow.

DRCCs (13) ensure the sufficiency of wind power with high probability, where P_w^A and P_w represent the available and integrated power of wind farms, respectively, where $1 - \varepsilon$ is a pre-specified risk threshold. We adopt a Wasserstein ball \mathcal{D} to describe the wind power ambiguity with

$$\mathcal{D} = \{ \mathbb{P} | d_W(\mathbb{P}, \mathbb{P}_N) \leq r \} \quad (14a)$$

$$d_W(\mathbb{P}, \mathbb{P}_N) = \inf_{(\omega, \omega_N) \sim (\mathbb{P}, \mathbb{P}_N)} \mathbb{E} [\| \omega - \omega_N \|], \quad (14b)$$

where \mathbb{P} represents an ambiguous distribution of the wind power, $\mathbb{P}_N = N(\mu_i, \tau, \sigma_i^2)$ is the Gaussian distribution with the mean μ and standard deviation σ , and r is the radius of \mathcal{D} .

The proposed formulation (5)–(13) is a mixed-integer non-linear program due to the DAEs and DRCCs. We recast them as tractable and computable forms in the next section.

III. SOLUTION ALGORITHM

We first derive an inner approximation for DAEs, and then reformulate it as well as the DRCCs as linear constraints.

A. Transformation of Frequency Security Metrics

To handle DAE frequency security constraints, we revisit the three metrics in (4). As analyzed in Section II.A, since the maximum RoCoF occurs at $t = 0$, constraint (4a) is equivalent to

$$2\overline{f} H_{sys,\tau} \geq \Delta P_{d,\tau}. \quad (15)$$

In addition, at the QSS, since $\Delta f(t)$ reaches a steady value, $\Delta f(t)|_{QSS}$ and $P_{(\cdot)}^{PR}(t)$ are unchanging. In other words, both $d\Delta f(t)/dt$ and $dP_{(\cdot)}^{PR}(t)/dt$ equal zero. It follows from (2)–(3) that (4c) is equivalent to

$$k_D P_d \overline{\Delta f_{err}} + G_{sys,\tau} (\overline{\Delta f_{err}} - \Delta f_{DB}) \geq \Delta P_{d,\tau} \quad (16a)$$

$$G_{sys,\tau} = \sum_i (G_{g,i} I_{g,i,\tau} + G_{w,i}), \quad (16b)$$

where G_{sys} represents the sum of droop factors.

Unlike RoCoF and QSS, $\Delta f(t)|_{nadir}$ is far more challenging to derive. Fortunately, the frequency nadir usually occurs beyond the dead band and so we can focus on the DAEs in (2)–(3). The next subsection derives an inner approximation using BPs.

B. DAE Approximation

We first introduce an approximation framework using BPs and then derive an inner approximation of the DAEs for computation.

1) BP approximation framework:

We restrict the functional form of the variables in the DAEs (2)–(3) using BP splines [36]. Specifically, if we restrict the functional form of a continuous-time function $F(t)$ to be cubic BPs, then

$$F(t) = \sum_{k=0}^3 F^{B,k} B_{3,k}(t) = (\mathbf{F}^B)^T \mathbf{B}_3(t), \quad t \in [0, 1] \quad (17)$$

where $B_{3,k}(t) := \binom{3}{k} t^k (1-t)^{3-k}$ for all $t \in [0, 1]$ and $k = 0, 1, 2, 3$ is a cubic BP, and $\mathbf{F}^B := [F^{B,0}, \dots, F^{B,3}]^T$ are the spline coefficients. This automatically guarantees the differentiability of $F(t)$ and allows us to compute its derivatives and integrals exactly or approximately. In particular,

$$\frac{dF(t)}{dt} = \frac{d(\mathbf{F}^B)^T \mathbf{B}_3(t)}{dt} = (\mathbf{W}\mathbf{F}^B)^T \mathbf{B}_2(t) \quad (18a)$$

$$\int_0^1 F(t) dt = \mathbf{1}^T \mathbf{F}^B / 4 \quad (18b)$$

$$\int_0^t F(t) dt = \int_0^t (\mathbf{F}^B)^T \mathbf{B}_3(t) dt \approx (\mathbf{F}^B)^T \mathbf{L}\mathbf{B}_3(t), \quad (18c)$$

$$F(t) = 0 \Leftrightarrow (\mathbf{F}^B)^T \mathbf{B}_3(t) = 0 \Leftrightarrow \mathbf{F}^B = 0 \quad (18d)$$

$$F(t) \leq 0 \Leftrightarrow (\mathbf{F}^B)^T \mathbf{B}_3(t) \leq 0 \Leftrightarrow \mathbf{J}\mathbf{F}^B \leq 0 \quad (18e)$$

where $B_{2,k}(t)$ represents quadratic BPs, and \mathbf{W} [36], \mathbf{L} [37], and \mathbf{J} [38] are matrices of known entries.

2) DAE approximation:

We apply the BP approximation framework to derive an inner approximation of the DAEs (2)–(3) and constraint (4b).

First, frequency dynamics are piecewise approximated using BP splines. Fig. 3 depicts an illustrative example. We divide

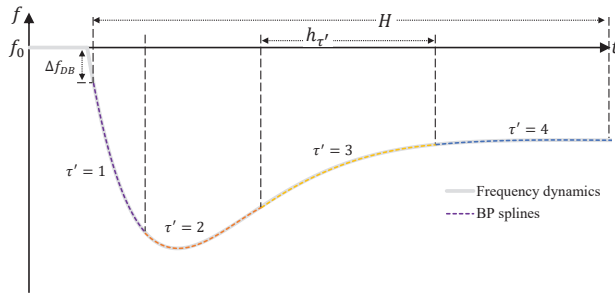


Fig. 3. BP spline-based frequency dynamics

the horizon of frequency dynamics, H , into several segments, each with a time length $h_{\tau'}$, where τ' is the index. For each segment, we normalize the time range as $[0, 1]$. Using BP splines, we approximate $\Delta f(t)$ in each segment τ' as

$$\Delta f_{\tau'}(t) = (\Delta \mathbf{f}_{\tau'}^B)^T \mathbf{B}_3(t), \quad t \in [0, 1] \quad (19)$$

where $\Delta \mathbf{f}^B$ consists of the spline coefficients. PFR dynamics $P_g^{PR}(t)$ and $P_w^{PR}(t)$ are similarly handled and $\mathbf{P}_g^{PR,B}$ and $\mathbf{P}_w^{PR,B}$ are the corresponding spline coefficients.

Second, we integrate both sides of (2a) from 0 to t to yield

$$\int_0^t \left[\frac{2H_{\text{sys}}}{h_{\tau'}} \frac{d\Delta f(t)}{dt} + k_D P_d \Delta f(t) \right] dt = \int_0^t [\Delta P_d - \Delta P_{\text{sys}}^{PR}(t)] dt, \quad (20)$$

which by (18) is equivalent to

$$\frac{2H_{\text{sys}}}{h_{\tau'}} (\Delta \mathbf{f}_{\tau'}^B - \Delta \mathbf{f}_{\tau',ini}^B) + k_D P_d \mathbf{L}^T \Delta \mathbf{f}_{\tau'}^B = \mathbf{L}^T (\Delta \mathbf{P}_d^B - \mathbf{P}_{\text{sys},\tau'}^{PR,B}) \quad (21a)$$

$$\Delta f_{\tau',ini}^B|_{\tau'=1} = \Delta f_{DB}, \quad \Delta f_{\tau',ini}^B|_{\tau'>1} = \Delta f_{\tau'-1}^B, \quad (21b)$$

where $\Delta \mathbf{f}_{\tau',ini}^B$ is the initial value of $\Delta \mathbf{f}_{\tau'}^B$ in period τ' and (21b) designates the initial condition for each period.

Similarly, (3) can be recast as

$$\mathbf{P}_{\text{sys},\tau'}^{PR,B} = \sum_i (\mathbf{P}_{g,i,\tau'}^{PR,B} + \mathbf{P}_{w,i,\tau'}^{PR,B}) \quad (22a)$$

$$\frac{T_{g,i}}{h_{\tau'}} (\mathbf{P}_{g,i,\tau'}^{PR,B} - \mathbf{P}_{g,i,\tau',ini}^{PR,B}) + \mathbf{L}^T \mathbf{P}_{g,i,\tau'}^{PR,B} = G_{g,i} I_{g,i} \mathbf{L}^T (\Delta \mathbf{f}_{\tau'}^B - \Delta \mathbf{f}_{DB}^B) \quad (22b)$$

$$P_{g,i,\tau',ini}^{PR,B,k}|_{\tau'=1} = 0, \quad P_{g,i,\tau',ini}^{PR,B,k}|_{\tau'>1} = P_{g,i,\tau'-1}^{PR,B,3} \quad (22c)$$

$$\mathbf{P}_{w,i,\tau'}^{PR,B} = G_{w,i} (\Delta \mathbf{f}_{\tau'}^B - \Delta \mathbf{f}_{DB}^B), \quad (22d)$$

where $\mathbf{P}_{w,i,\tau',ini}^{PR,B}$ is the initial value of $\mathbf{P}_{w,i,\tau'}^{PR,B}$ in period τ' .

Finally, by (18e), constraints (4b) and (9c) are respectively implied by

$$\mathbf{J} \Delta \mathbf{f}_{\tau'}^B \leq \overline{\Delta f} \quad (23)$$

$$\text{and } \begin{cases} \mathbf{J} \mathbf{P}_{g,i,\tau',\tau'}^{PR,B} \leq R_{g,i,\tau}^{PR} \\ \mathbf{J} \mathbf{P}_{w,i,\tau',\tau'}^{PR,B} \leq R_{w,i,\tau}^{PR} \end{cases} \quad (24)$$

Consequently, we inner approximate the DAE frequency security constraints by general algebraic constraints (15), (16), and (21)–(24).

C. Linearization

We reformulate the bilinear terms $H_{\text{sys}} \Delta \mathbf{f}_{\tau'}^B$ in (21a), $I_{g,i} \Delta \mathbf{f}_{\tau'}^B$ in (22b), and $G_{w,i} \Delta \mathbf{f}_{\tau'}^B$ in (22d) as linear forms for tractable computation. In what follows, we linearize $G_{w,i} \Delta \mathbf{f}_{\tau'}^B$ as an example, and the linearization of other bilinear terms can be conducted similarly.

1) *Binary expansion*: Assuming that the droop factor G_w can only be adjusted discretely with a minimum stepsize ΔG_w [39], we encode G_w using binary decision variables ω_k as

$$G_w = \sum_{k=0}^{N_{BE}-1} \omega_k 2^k \Delta G_w, \quad \omega_k \in \{0, 1\}, \quad (25)$$

where N_{BE} is a pre-specified number for ω_k to adjust the granularity of the binary expansion.

2) *Big-M method*: With the above binary expansion, the bilinear term $G_w \Delta \mathbf{f}_{\tau'}^B$ can be rewritten as $\Delta \mathbf{f}_{\tau'}^B \sum_k \omega_k 2^k \Delta G_w$. Then, through the big-M method, the new bilinear terms $\alpha_{k,\tau'} = \omega_k \Delta \mathbf{f}_{\tau'}^B$ can be linearized as

$$-M \omega_k \leq \alpha_{k,\tau'} \leq M \omega_k \quad (26a)$$

$$-M(1 - \omega_k) + \Delta \mathbf{f}_{\tau'}^B \leq \alpha_{k,\tau'} \leq \Delta \mathbf{f}_{\tau'}^B + M(1 - \omega_k). \quad (26b)$$

3) *DRCC Reformulation*: We follow [32] to recast the DRCC (13) as

$$P_{w,i,\tau} + R_{w,i,\tau}^{PR} \leq \mu_{i,\tau} - c_p \sigma_{i,\tau} \quad (27)$$

where c_p is a parameter that only depends on ε and r and can be computed beforehand.

We have recast the proposed frequency-secured UC formulation (5)–(13) as a mixed-integer linear program, which can be directly computed by off-the-shelf solvers.

IV. CASE STUDY

We first demonstrate the tightness of the BP approximation. Then, using the IEEE 6-bus system, we analyze frequency security, influence of the dead band, variable droop factors, and parameter settings of the DRCCs. Finally, we demonstrate the scalability of our approach using an IEEE 118-bus system.

A. Tightness of Frequency Dynamics

We demonstrate the tightness of the BP approximation (21)–(22) in evaluating the nadir. We consider three thermal units and a wind farm and their parameters are the same as in the 6-bus system in Section IV-B (see Table II), except that for now we fix the droop factor of the wind farm at 20 MW/Hz. We illustrate the corresponding SFR model in Fig. 4.

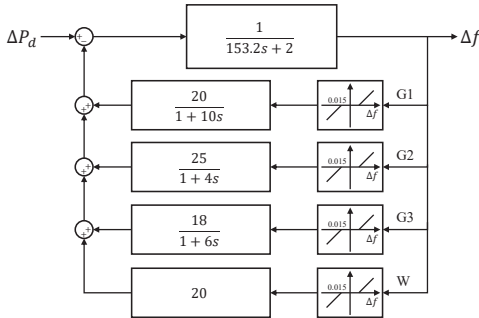


Fig. 4. SFR model with three thermal units and a wind farm

We consider a power imbalance of 20MW and the frequency dynamics in the subsequent 30s-horizon. Fig. 5 depicts the frequency dynamics obtained from the BP approximation and those obtained from numerical simulation (by Simulink). In this implementation, we divide the 30s-horizon evenly into N segments and compare the results with different N . From Fig. 5, we observe that when $N = 1$, BP performs poorly in approximating the frequency dynamics and the estimated nadir is higher than the true nadir. But as N increases, each period shortens and the performance of BP quickly improves. We report the estimated nadir values and their relative errors in Table I.

TABLE I
ESTIMATED NADIR VALUES AND THEIR RELATIVE ERRORS

	Simulink	BP approximation		
		$N = 1$	$N = 2$	$N = 4$
Nadir value (Hz)	-0.388385	-0.375927	-0.389262	-0.389182
Relative error	\	3.21%	0.23%	0.20%

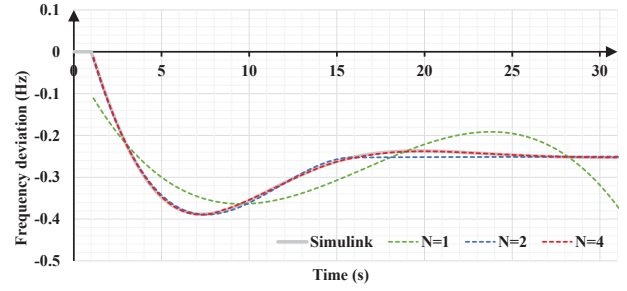


Fig. 5. Frequency dynamics from BP approximation vs. from Simulink

In addition, considering that frequency dynamics are accumulated temporally, we can divide the horizon unevenly such that we have shorter segments before the nadir for a more accurate estimate of $\Delta f(t)|_{\text{nadir}}$. To this end, we divide the 30s-horizon into 4 segments with 10%, 20%, 30%, and 40% of the horizon, respectively. We depict the frequency dynamics approximation in this case in Fig. 6. From this figure, we observe that the BP approximation is highly accurate and the relative error in estimating $\Delta f(t)|_{\text{nadir}}$ is lower than 0.04%. This validates the tightness of the proposed method.

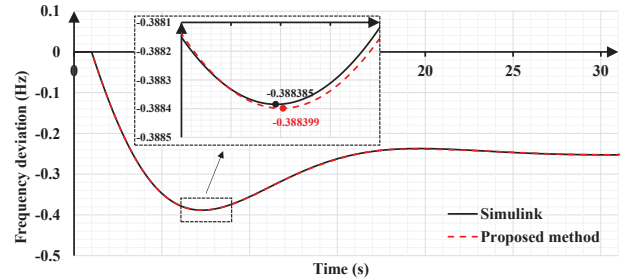


Fig. 6. BP approximation with an uneven division of the horizon

B. 6-Bus System

Next, we use the IEEE 6-bus system for analysis. The system includes 3 thermal units (G1, G2, and G3) and a newly-added wind farm (W). The load curve and the predicted available wind power are depicted in Fig. 7. The maximum total load is 210MW. The standard deviation of wind power prediction is set as 5% of the predicted value. The risk level in chance constraints is set as 10% and the radius of the Wasserstein ball for DRCC is set as 0.01.

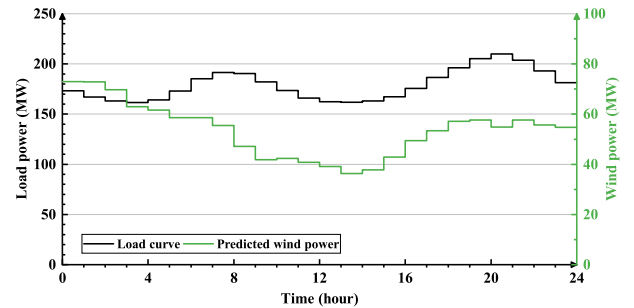


Fig. 7. Load curve and predicted wind power

Table II displays the main technical parameters of thermal units and the wind farm. The fuel cost coefficients are the

same as in [35]. The droop factor of the wind farm is set as 20 MW/Hz by default and can be adjusted from 10 MW/Hz to 25 MW/Hz with a stepsize of 5 MW/Hz. The nominal frequency is 50 Hz and the dead band is set as 0.015 Hz [22]. The cost coefficients of PFR reserves are 15 \$/MWh and 5 \$/MWh for thermal units and the wind farm, respectively. In each hour, we consider a sudden power imbalance of 10% total load. We set the load damping factor as 1% total load per Hz, the maximum admitted RoCoF as 0.5 Hz/s, and the maximum admitted frequency deviation at the nadir and at the QSS as 0.5 Hz and 0.3 Hz, respectively. We consider a 30s-horizon of frequency dynamics and divide it into 4 segments with 10%, 20%, 30%, and 40% of the horizon, respectively.

TABLE II
MAIN TECHNICAL PARAMETERS OF THE 6-BUS SYSTEM

Units	G1	G2	G3	W
Capacity (MW)	200	150	180	80
Minimum generation (MW)	60	45	54	\
Inertia constant (s)	8	5	6	5
Response constant (s)	10	4	6	0
Droop factor (MW/Hz)	20	25	18	10~25

1) *Baseline Results:* With the above parameter settings, we compare the following two UC formulations:

- (**Case 1**) without frequency security constraints; and
- (**Case 2**) with frequency security constraints (4) and (9).

We report the optimal UC solutions and generation schedules of these two cases in Figs. 8–9, respectively, and their performance details in Table III.

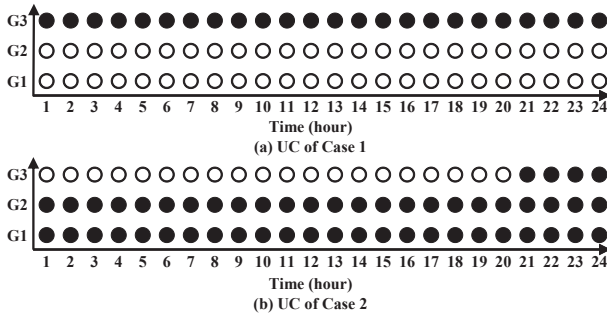
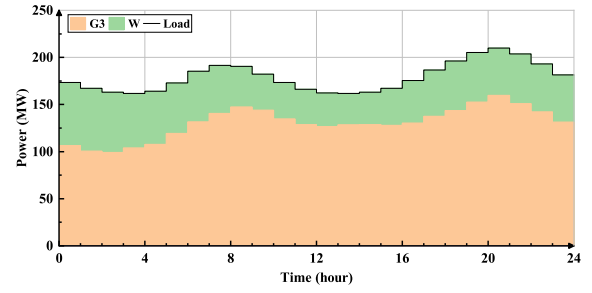


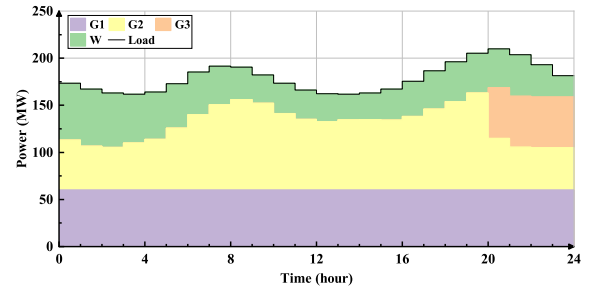
Fig. 8. Optimal UC in Cases 1 and 2

TABLE III
DETAILED COMPARISON BETWEEN CASES 1 AND 2

Comparison terms	Case 1	Case 2
Start-up & shut-down cost (\$)	0	5400
Fuel cost of thermal units (\$)	42668.53	49040.87
PFR reserve cost of thermal units (\$)	0	5171.99
PFR reserve cost of wind farm (\$)	0	919.69
Total cost (\$)	42668.53	60532.55
Total PFR reserve of thermal units (MWh)	0	344.80
Total PFR reserve of wind farm (MWh)	0	183.94
Maximum RoCoF (Hz/s)	0.3547	0.1866
Maximum Δf at the nadir (Hz)	0.7065	0.4578
Maximum Δf at the quasi-steady state (Hz)	0.5379	0.2995
Computation time (s)	8.22	38.42



(a) Case 1



(b) Case 2

Fig. 9. Generation schedule in Cases 1 and 2

From Figs. 8–9 and Table III, we observe that in Case 1, only G3 is online. For this case, we simulate the frequency dynamics under power imbalance and find that in hour 21, the frequency deviation reaches 0.7065 Hz at the nadir and reaches 0.5379 Hz at the QSS, which exceeds the frequency security limits (0.5 Hz and 0.3 Hz, respectively). The frequency dynamics of hour 21 in Case 1 are provided in Fig. 10.

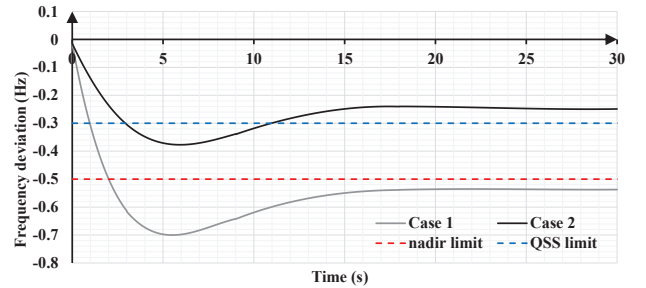


Fig. 10. Frequency dynamics of hour 21 in Cases 1 and 2

In contrast, in Case 2, G1 and G2 are always online and G3 is started up in hour 21, which provides more inertia and PFR capacity than those in Case 1 (see Fig. 11). We depict the PFR reserve and the droop factor of the wind farm in Fig. 12. From this figure, we observe that most wind power is integrated for power supply or reserved for frequency support, and a only small portion of wind power is curtailed in the last two hours. In addition, the droop factor varies across different hours, which will be further discussed later. As a consequence of more units online and more PFR reserves from both the thermal units and the wind farm, in Case 2, the maximum frequency deviation becomes 0.4578 Hz at the nadir and 0.2995 Hz at the QSS, significantly lower than those in Case 1. Note that, since G3 is online from hour 21 in Case 2, the maximum nadir frequency deviation occurs in hour 20

and the maximum QSS frequency deviation occurs in hour 11. We also depict the frequency dynamics of hour 21 in Case 2 in Fig. 10 for comparison and the corresponding PFR power dynamics in Fig. 13. The above analyses demonstrate that the proposed model can effectively protect frequency security.

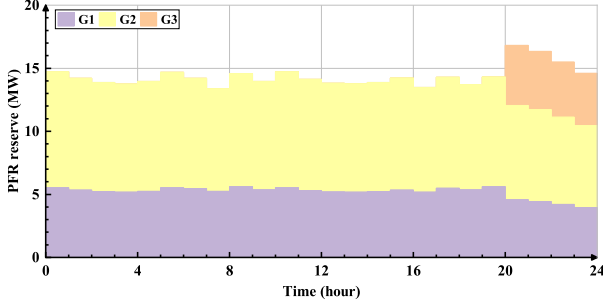


Fig. 11. PFR reserves of thermal units in Case 2

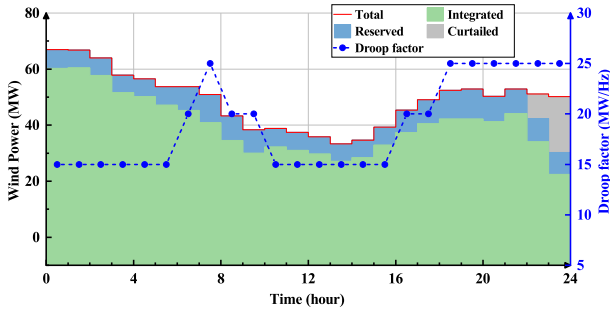


Fig. 12. Operation of the wind farm in Case 2

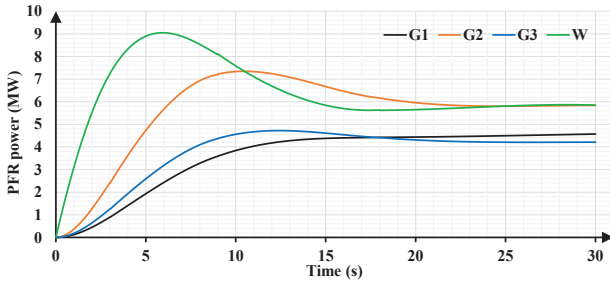


Fig. 13. PFR power dynamics of hour 21 in Case 2

2) *Impact of the Dead Band*: To evaluate the value of modeling the dead band in frequency security, we consider a third UC formulation:

(Case 3) without considering the dead band in Case 2.

We report the optimal UC solution in Case 3 in Fig. 14 and the performance details in Table IV.

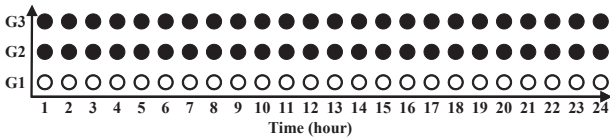


Fig. 14. Optimal UC in Case 3

From Fig. 14 and Table IV, we observe that in Case 3, G2 and G3 remain online while G1 remains offline across all periods. Because the more economic G2 and G3 are utilized, the total cost in Case 3 is lower than that in Case 2. However,

TABLE IV
DETAILED COMPARISON BETWEEN CASES 3 AND 2

Comparison terms	Case 3	Case 2
Start-up & shut-down cost (\$)	0	5400
Fuel cost of thermal units (\$)	47718.70	49040.87
PFR reserve cost of thermal units (\$)	4712.09	5171.99
PFR reserve cost of wind farm (\$)	1033.06	919.69
Total cost (\$)	53463.85	60532.55
Maximum RoCoF (Hz/s)	0.2354	0.1866
Maximum Δf at the nadir (Hz)	0.4662	0.4578
Maximum Δf at the quasi-steady state (Hz)	0.3141	0.2995

ignoring the dead band causes undesirable frequency dynamics. From Table IV, we observe that the maximum $\Delta f(t)|_{QSS}$ in Case 3 reaches 0.3141 Hz, exceeding frequency security limit (0.3 Hz). This highlights the necessity of considering the dead band in frequency-secured UC.

3) *Benefits of Variable Droop Factors*: To evaluate the benefit of adopting variable droop factors of the wind farm, as opposed of constant droop factors, we consider a fourth UC formulation:

(Case 4) fixing the droop factor in Case 2 at 20 MW/Hz.

We report the optimal UC solution in Case 4 in Fig. 15 and the performance details in Table V.

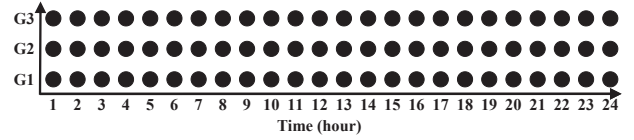


Fig. 15. Optimal UC in Case 4

TABLE V
DETAILED COMPARISON BETWEEN CASES 4 AND 2

Comparison terms	Case 4	Case 2
Start-up & shut-down cost (\$)	0	5400
Fuel cost of thermal units (\$)	59198.07	49040.87
PFR reserve cost of thermal units (\$)	5595.82	5171.99
PFR reserve cost of wind farm (\$)	809.83	919.69
Total cost (\$)	65603.72	60532.55
Maximum RoCoF (Hz/s)	0.1371	0.1866
Maximum Δf at the nadir (Hz)	0.4087	0.4578
Maximum Δf at the quasi-steady state (Hz)	0.2614	0.2995

From Fig. 15 and Table V, we observe that in Case 4, all thermal units remain online all the time and the total cost is higher than that in Case 2. We provide the PFR reserve and droop factors of the wind farm in Case 4 in Fig. 16. Comparing Figs. 16 and 12, we observe that much more wind curtailment occurs in Case 4. The reason is analyzed in the following. In Case 4, if we replace its UC with that in Case 2 while keeping the droop factors unchanged, $\Delta f(t)|_{QSS}$ would reach 0.3007 Hz at hour 8 and 0.3207 Hz at hour 20 (see Fig. 17), which exceed the frequency security limit (0.3 Hz). Hence, in Case 4, G3 needs to be online to reduce $\Delta f(t)|_{QSS}$, and consequently, much wind power needs to be curtailed to satisfy the minimum generation limits of the thermal units. In contrast, in Case 2, we reduce $\Delta f(t)|_{QSS}$ by increasing the droop factor (such as in hours 8 and 20; see Fig. 12), which avoids putting G3 online and reduces the total cost by 7.69%. These results demonstrate

that variable droop factors can improve the coordination of different frequency resources for higher operational economy.

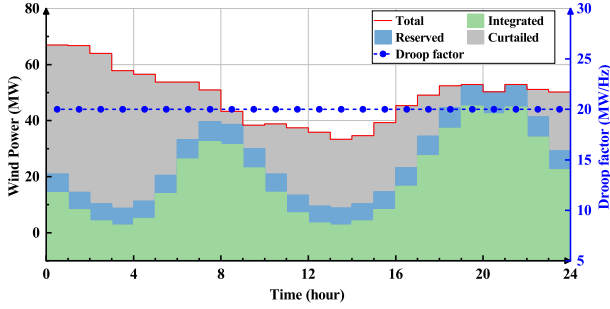


Fig. 16. Operation of the wind farm in Case 4

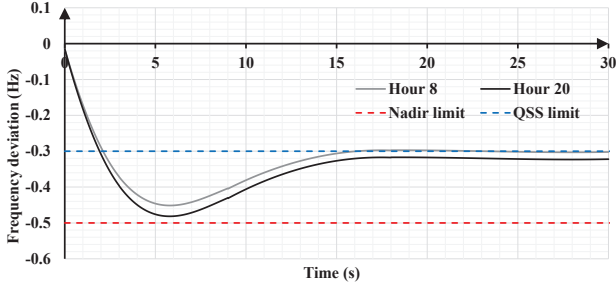
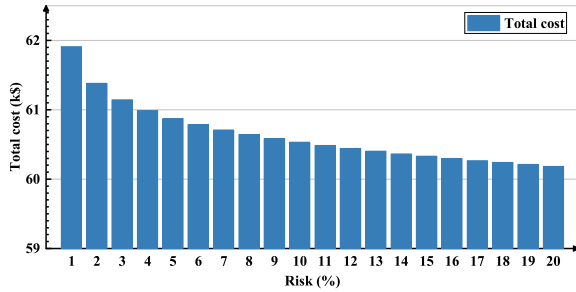
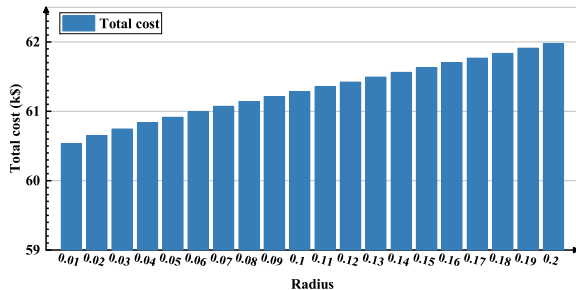


Fig. 17. Frequency dynamics of hour 8 and hour 20

4) *DRCC Sensitivity Analysis*: We vary the risk level ε and the Wasserstein ball radius r to see their impacts on the total cost of the frequency-secured UC model. The results are reported in Fig. 18. This figure provides clear trade-offs among operational economy, risk attitude, and robustness, which can better assist the system operators. In particular, the total cost is more sensitive to the risk level than it is to the Wasserstein ball radius, especially when ε is small (or equivalently, when $1 - \varepsilon$ is close to 1). On the other hand, when ε exceeds 0.1, the total cost depends almost linearly in ε and r .



(a) Risk level ε



(b) Radius r of the Wasserstein ball

Fig. 18. DRCC sensitivity analysis

C. Scalability Test in IEEE 118-Bus System

We evaluate the scalability of our approach using the IEEE 118-bus system, which includes 54 thermal units and a 4242 MW of maximum total load. We follow [22] on the frequency-related parameters. We scale up the capacity of the wind farm to 800 MW and accordingly the wind power and the range of the droop factors. The results are reported in Table VI.

TABLE VI
RESULTS IN IEEE 118-BUS SYSTEM

Comparison terms	Case 1	Case 2
Operation cost of thermal units (k\$)	2184.18	2394.85
PFR reserve cost of thermal units (k\$)	0	155.65
PFR reserve cost of wind farm (k\$)	0	9.81
Total cost (k\$)	2184.18	2560.32
Maximum RoCoF (Hz/s)	0.2598	0.1696
Maximum Δf at the nadir (Hz)	0.7748	0.4318
Maximum Δf at the quasi-steady state (Hz)	0.4950	0.1935
Computation time (s)	49.98	2472

From Table VI, we observe that in Case 1, the frequency deviation of hour 21 reaches 0.7748 Hz at the nadir and reaches 0.4950 Hz at the QSS, exceeding the frequency security limits. In contrast, in Case 2, all frequency security limits are respected. (see Fig. 19). Fig. 20 provides the PFR power in Case 2. These results demonstrate the effectiveness and scalability of the proposed method in protecting frequency security in larger-sized systems.

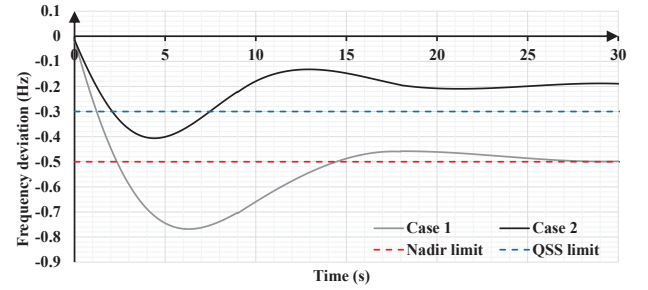


Fig. 19. Comparison of frequency dynamics in IEEE 118-bus system

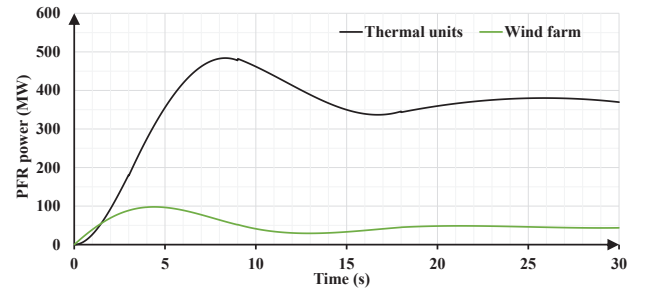


Fig. 20. PFR power dynamics of Case 2 in IEEE 118-bus system

V. CONCLUSIONS

This paper proposed a frequency-secured UC model considering frequency dynamics, wind power uncertainty, and variable droop factors. In this model, we incorporated frequency dynamics using DAEs and considered the dead band. Then, we derived an inner approximation of the DAEs using

BP splines and linearization techniques. A comparison with Simulink demonstrated the tightness of the BP approximation in depicting frequency dynamics and evaluating the frequency deviation at the nadir, with a relative error below 0.04%. Extensive case studies based on IEEE 6-bus and 118-bus systems demonstrated the effectiveness of the proposed model in deciding UC and PFR reserves for frequency security, the necessity of considering the dead band in frequency dynamics, and the value of using variable droop factors of the wind farms in improving the coordination among different frequency support resources, which can help reduce the total cost significantly.

REFERENCES

- [1] IRENA, "Renewable energy statistics 2021," International Renewable Energy Agency, Tech. Rep., 2021.
- [2] L. Xie, P. M. S. Carvalho, L. A. F. M. Ferreira, J. Liu, B. H. Krogh, N. Popli, and M. D. Ilic, "Wind integration in power systems: Operational challenges and possible solutions," *Proceedings of the IEEE*, vol. 99, no. 1, pp. 214–232, 2011.
- [3] H. D. Tafti, Q. Wang, C. D. Townsend, J. Pou, and G. Konstantinou, "Global flexible power point tracking in photovoltaic systems under partial shading conditions," *IEEE transactions on power electronics*, vol. 37, no. 9, pp. 11 332–11 341, 2022.
- [4] I. Serban and C. Marinescu, "Control strategy of three-phase battery energy storage systems for frequency support in microgrids and with uninterrupted supply of local loads," *IEEE transactions on power electronics*, vol. 29, no. 9, pp. 5010–5020, 2014.
- [5] J. Zhu, C. D. Booth, G. P. Adam, A. J. Roscoe, and C. G. Bright, "Inertia emulation control strategy for vsc-hvdc transmission systems," *IEEE transactions on power systems*, vol. 28, no. 2, 2013.
- [6] J. Rocabert, A. Luna, F. Blaabjerg, and P. R. Iiguez, "Control of power converters in ac microgrids," *IEEE Transactions on Power Electronics*, vol. 27, no. 11, pp. 4734–4749, 2012.
- [7] H. DehghaniTafti, G. Konstantinou, J. Fletcher, L. Callegaro, G. Farivar, and J. Pou, "Control of distributed photovoltaic inverters for frequency support and system recovery," *IEEE transactions on power electronics*, vol. 37, no. 4, pp. 4742–4750, 2022.
- [8] J. F. Restrepo and F. D. Galiana, "Unit commitment with primary frequency regulation constraints," *IEEE Transactions on Power Systems*, vol. 20, no. 4, pp. 1836–1842, 2005.
- [9] F. D. Galiana, F. Bouffard, J. M. Arroyo, and J. F. Restrepo, "Scheduling and pricing of coupled energy and primary, secondary, and tertiary reserves," *Proceedings of the IEEE*, vol. 93, no. 11, pp. 1970–1983, 2005.
- [10] K. V. Vidyandandan and N. Senroy, "Primary frequency regulation by deloaded wind turbines using variable droop," *IEEE Transactions on Power Systems*, vol. 28, no. 2, pp. 837–846, 2013.
- [11] Y.-Y. Lee and R. Baldick, "A frequency-constrained stochastic economic dispatch model," *IEEE transactions on power systems*, vol. 28, no. 3, pp. 2301–2312, 2013.
- [12] Y. Wen, W. Li, G. Huang, and X. Liu, "Frequency dynamics constrained unit commitment with battery energy storage," *IEEE Transactions on Power Systems*, vol. 31, no. 6, pp. 5115–5125, 2016.
- [13] L. Badesa, F. Teng, and G. Strbac, "Simultaneous scheduling of multiple frequency services in stochastic unit commitment," *IEEE transactions on power systems*, vol. 34, no. 5, pp. 3858–3868, 2019.
- [14] K. Li, H. Guo, X. Fang, S. Liu, F. Teng, and Q. Chen, "Market mechanism design of inertia and primary frequency response with consideration of energy market," *IEEE Transactions on Power Systems*, early access.
- [15] L. Badesa, F. Teng, and G. Strbac, "Conditions for regional frequency stability in power system scheduling-part i: Theory," *IEEE transactions on power systems*, vol. 36, no. 6, pp. 5558–5566, 2021.
- [16] —, "Conditions for regional frequency stability in power system scheduling—part ii: Application to unit commitment," *IEEE Transactions on Power Systems*, vol. 36, no. 6, pp. 5567–5577, 2021.
- [17] X. Zhao, H. Wei, J. Qi, P. Li, and X. Bai, "Frequency stability constrained optimal power flow incorporating differential algebraic equations of governor dynamics," *IEEE Transactions on Power Systems*, vol. 36, no. 3, pp. 1666–1676, 2021.
- [18] G. Kou, P. Markham, S. Hadley, T. King, and Y. Liu, "Impact of governor deadband on frequency response of the u.s. eastern interconnection," *IEEE Transactions on Smart Grid*, vol. 7, no. 3, pp. 1368–1377, 2016.
- [19] M. Liu, F. Bizzarri, A. M. Brambilla, and F. Milano, "On the impact of the dead-band of power system stabilizers and frequency regulation on power system stability," *IEEE transactions on power systems*, vol. 34, no. 5, pp. 3977–3979, 2019.
- [20] Z. Zhang, M. Zhou, Z. Wu, S. Liu, Z. Guo, and G. Li, "A frequency security constrained scheduling approach considering wind farm providing frequency support and reserve," *IEEE Transactions on Sustainable Energy*, vol. 13, no. 2, pp. 1086–1100, 2022.
- [21] H. Li, Y. Qiao, Z. Lu, B. Zhang, and F. Teng, "Frequency-constrained stochastic planning towards a high renewable target considering frequency response support from wind power," *IEEE Transactions on Power Systems*, vol. 36, no. 5, pp. 4632–4644, 2021.
- [22] L. Yang, Y. Xu, J. Zhou, and H. Sun, "Distributionally robust frequency constrained scheduling for an integrated electricity-gas system," *IEEE Transactions on Smart Grid*, vol. 13, no. 4, pp. 2730–2743, 2022.
- [23] Z. Chu, N. Zhang, and F. Teng, "Frequency-constrained resilient scheduling of microgrid: A distributionally robust approach," *IEEE Transactions on Smart Grid*, vol. 12, no. 6, pp. 4914–4925, 2021.
- [24] H. Ahmadi and H. Ghasemi, "Security-constrained unit commitment with linearized system frequency limit constraints," *IEEE transactions on power systems*, vol. 29, no. 4, pp. 1536–1545, 2014.
- [25] Z. Zhang, E. Du, F. Teng, N. Zhang, and C. Kang, "Modeling frequency dynamics in unit commitment with a high share of renewable energy," *IEEE transactions on power systems*, vol. 35, no. 6, pp. 4383–4395, 2020.
- [26] R. Jiang, J. Wang, and Y. Guan, "Robust unit commitment with wind power and pumped storage hydro," *IEEE Transactions on Power Systems*, vol. 27, no. 2, pp. 800–810, 2012.
- [27] T. Ding, Z. Zeng, M. Qu, J. P. S. Catalao, and M. Shahidehpour, "Two-stage chance-constrained stochastic thermal unit commitment for optimal provision of virtual inertia in wind-storage systems," *IEEE Transactions on Power Systems*, vol. 36, no. 4, pp. 3520–3530, 2021.
- [28] S. Zheng, K. Liao, J. Yang, and Z. He, "Optimal scheduling of distribution network with autonomous microgrids: Frequency security constraints and uncertainties," *IEEE Transactions on Sustainable Energy*, early access.
- [29] Y. Zhang, S. Shen, and J. Mathieu, "Distributionally robust chance-constrained optimal power flow with uncertain renewables and uncertain reserves provided by loads," *IEEE Transactions on Power Systems*, vol. 32, no. 2, pp. 1378–1388, 2017.
- [30] L. Jiang, Z. Bie, T. Long, X. Wang, H. Xie, and G. Li, "A post-event generator start-up strategy for renewable penetrated transmission system considering dynamic frequency regulation," *IEEE Transactions on Sustainable Energy*, early access.
- [31] B. Li, R. Jiang, and J. L. Mathieu, "Ambiguous risk constraints with moment and unimodality information," *Mathematical Programming*, vol. 173, no. 1, pp. 151–192, 2019.
- [32] H. Shen and R. Jiang, "Convex chance-constrained programs with wasserstein ambiguity," *arXiv preprint arXiv:2111.02486*, 2021.
- [33] —, "Wasserstein two-sided chance constraints with an application to optimal power flow," *arXiv preprint arXiv:2204.00191*, 2022.
- [34] Y. Yuan, Y. Zhang, J. Wang, Z. Liu, and Z. Chen, "Enhanced frequency-constrained unit commitment considering variable-droop frequency control from converter-based generator," *IEEE transactions on power systems*, early access.
- [35] B. Zhou, J. Fang, X. Ai, Y. Zhang, W. Yao, Z. Chen, and J. Wen, "Partial-dimensional correlation-aided convex-hull uncertainty set for robust unit commitment," *IEEE Transactions on Power Systems*, early access.
- [36] M. Parvania and A. Scaglione, "Unit commitment with continuous-time generation and ramping trajectory models," *IEEE Transactions on Power Systems*, vol. 31, no. 4, pp. 3169–3178, 2016.
- [37] C. Zheng, J. Fang, S. Wang, X. Ai, Z. Liu, and Z. Chen, "Energy flow optimization of integrated gas and power systems in continuous time and space," *IEEE Transactions on Smart Grid*, vol. 12, no. 3, pp. 2611–2624, 2021.
- [38] B. Zhou, J. Fang, X. Ai, W. Yao, and J. Wen, "Flexibility-enhanced continuous-time scheduling of power system under wind uncertainties," *IEEE Transactions on Sustainable Energy*, vol. 12, no. 4, pp. 2306–2320, 2021.
- [39] B. Zhou, J. Fang, X. Ai, S. Cui, W. Yao, Z. Chen, and J. Wen, "Storage right-based hybrid discrete-time and continuous-time flexibility trading between energy storage station and renewable power plants," *IEEE Transactions on Sustainable Energy*, early access.